SUPPLEMENTARY MATERIALS: Regularization with Optimal Space-Time Priors*

Tatiana A. Bubba†, Tommi Heikkilä‡, Demetrio Labate§, and Luca Ratti¶

This supplementary material contains additional plots and reconstruction images related to the numerical tests in section 4.

Figure SM1 and Figure SM2 contain the expected Bregman distance $\mathbb{E}\left[D_{\boldsymbol{R}}(\boldsymbol{f}^{\delta}_{\alpha,N}, \boldsymbol{f}^{\dagger})\right]$ values as a function of N for the two data sets (simulated cartoon phantom and measured STEMPO phantom), respectively in the theoretically justified case of $p = 3/2$. The resulting slopes are also reported in Table 1 in all test scenarios.

Similarly, Figure SM3 and Figure SM4 contain the values of the expected Bregman distance $\mathbb{E}\left[D_{\boldsymbol{R}}(\boldsymbol{f}^{\delta}_{\alpha,N}, \boldsymbol{f}^{\dagger})\right]$ as a function of N for the two data sets (simulated cartoon phantom and measured STEMPO phantom), respectively for $p = 1$. The resulting slopes are also reported in Table 1.

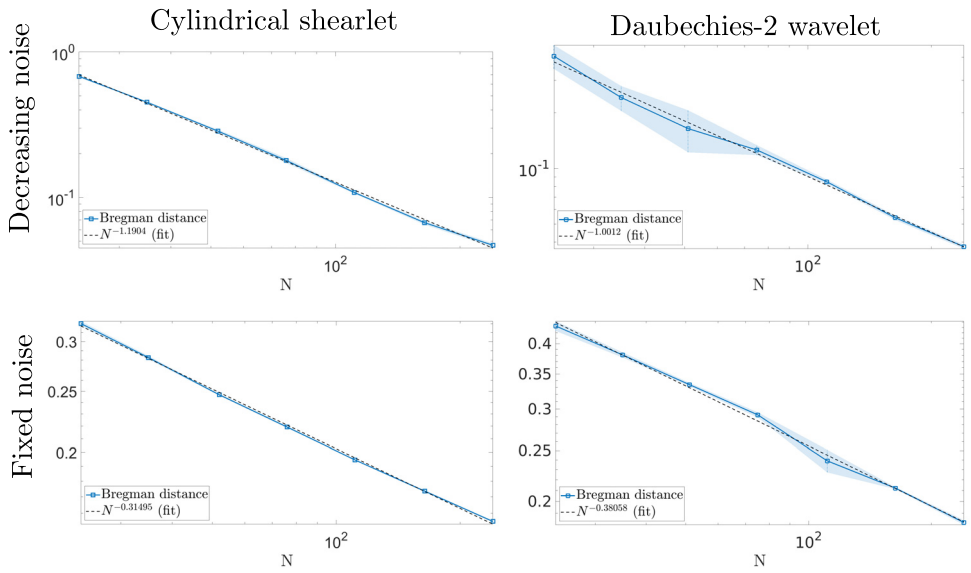

Figure SM1. *Approximate decay of the expected value of the Bregman distance for the simulated cartoon phantom, using cylindrical shearlet-based regularization (left column) wavelets-based regularization (right column) with $p = 3/2$. Top row: decreasing noise regime. Bottom row: fixed noise regime. Each N is averaged from 5 samples.*

*Supplementary material for SIIMS MS#M166192.
https://doi.org/10.1137/24M1661923

†Department of Mathematics and Computer Science, University of Ferrara, Ferrara, Italy (tatiana.bubba@unife.it).
‡School of Engineering Sciences, LUT University, Lappeenranta, Finland (tommi.heikkila@lut.fi).
§Department of Mathematics, University of Houston, Houston, TX 77204-3008 USA (dlabate@math.uh.edu).
¶Department of Mathematics, University of Bologna, Bologna, Italy (luca.ratti5@unibo.it).

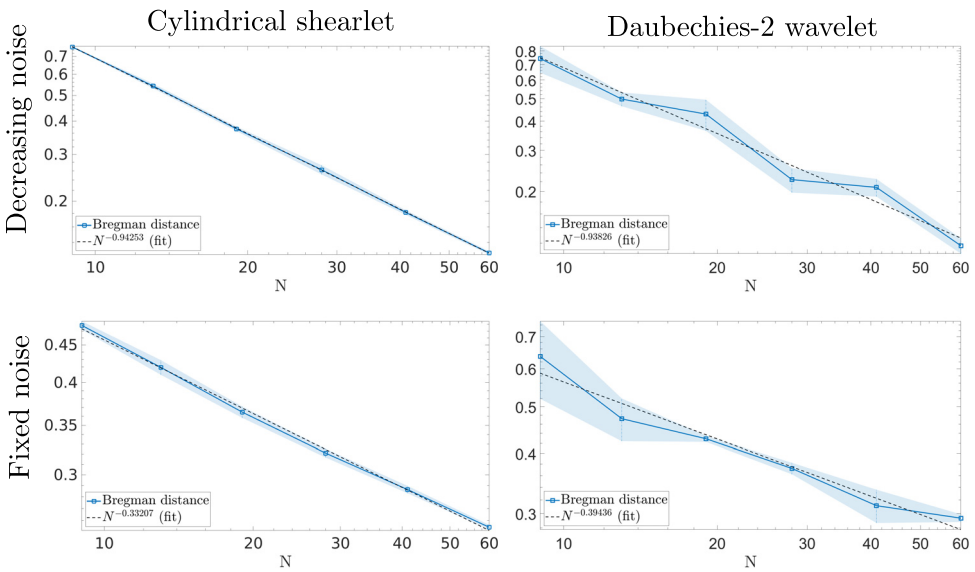

Figure SM2. *Approximate decay of the expected value of the Bregman distance for the measured STEMPO data, using cylindrical shearlet-based regularization (left column) wavelets-based regularization (right column) with $p = 3/2$. Top row: decreasing noise regime. Bottom row: fixed noise regime. Each N is averaged from 5 samples.*

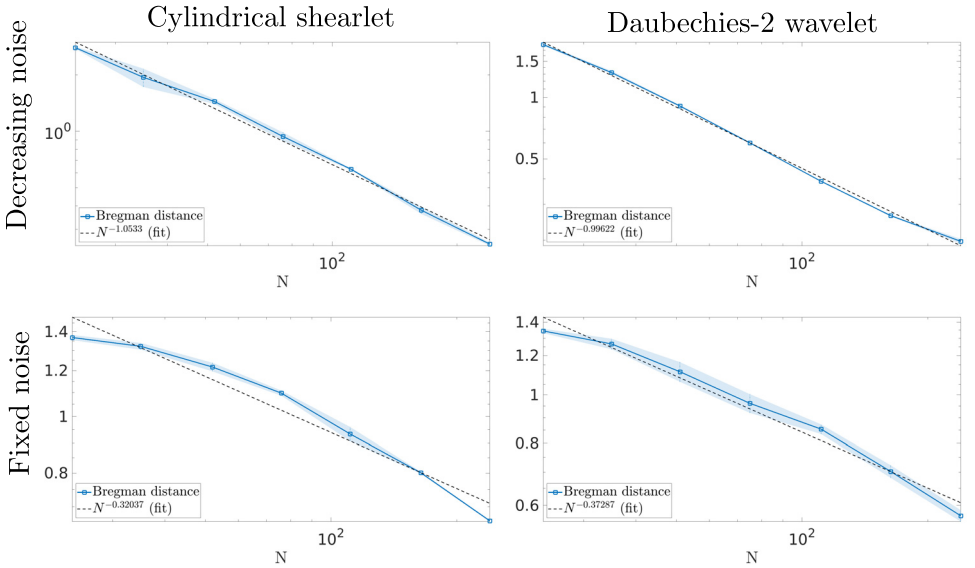

Figure SM3. *Approximate decay of the expected value of the Bregman distance for the simulated cartoon phantom, using cylindrical shearlet-based regularization (left column) wavelets-based regularization (right column) with $p = 1$. Top row: decreasing noise regime. Bottom row: fixed noise regime. Each N is averaged from 5 samples.*

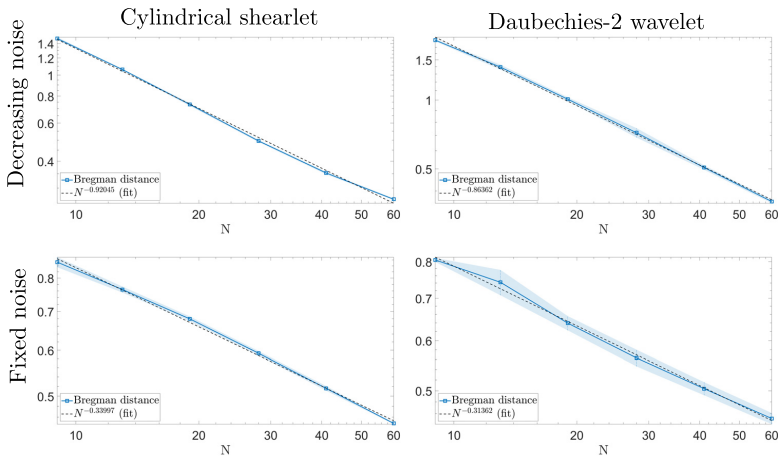

Figure SM4. *Approximate decay of the expected value of the Bregman distance for the STEMPO data, using cylindrical shearlet-based regularization (left column) wavelets-based regularization (right column) with* $p = 1$*. Top row: decreasing noise regime. Bottom row: fixed noise regime. Each* N *is averaged from* 5 *samples.*

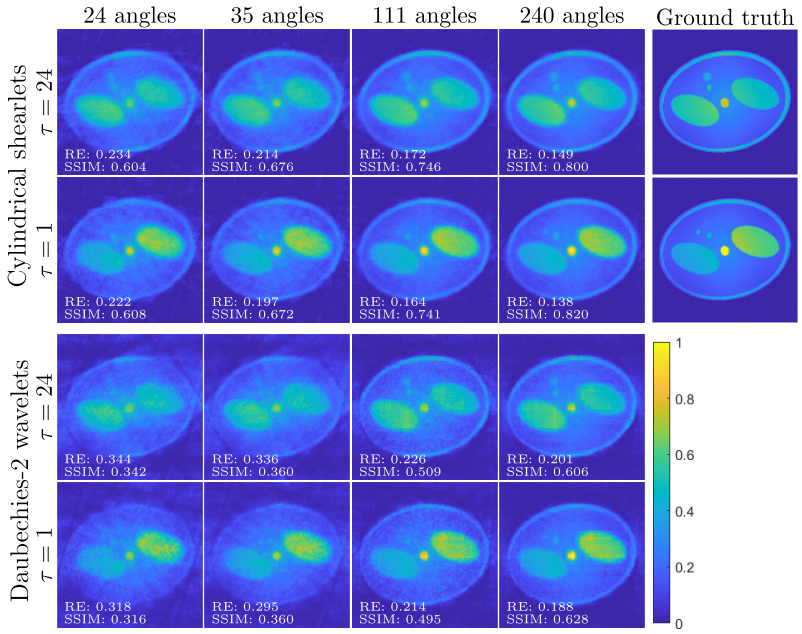

Figure SM5. *Cylindrical shearlet and wavelet reconstructions from selected time steps and angular samples, fixed noise,* $p = \frac{3}{2}$*. Simulated Cartoon data. The relative* ℓ^2 *error and SSIM values are also reported.*

In Figure SM5 we show some reconstructions from the simulated cartoon data for the fixed noise scenario and $p = \frac{3}{2}$ (using both cylindrical shearlets and wavelets). Moreover the relative ℓ^2 error and Structure Similarity Index Metric (SSIM) of the respective time frame is reported.

Finally, in Figure SM6 we have included additional pixelwise variance images similar to Figure 7, but with more projection counts N.

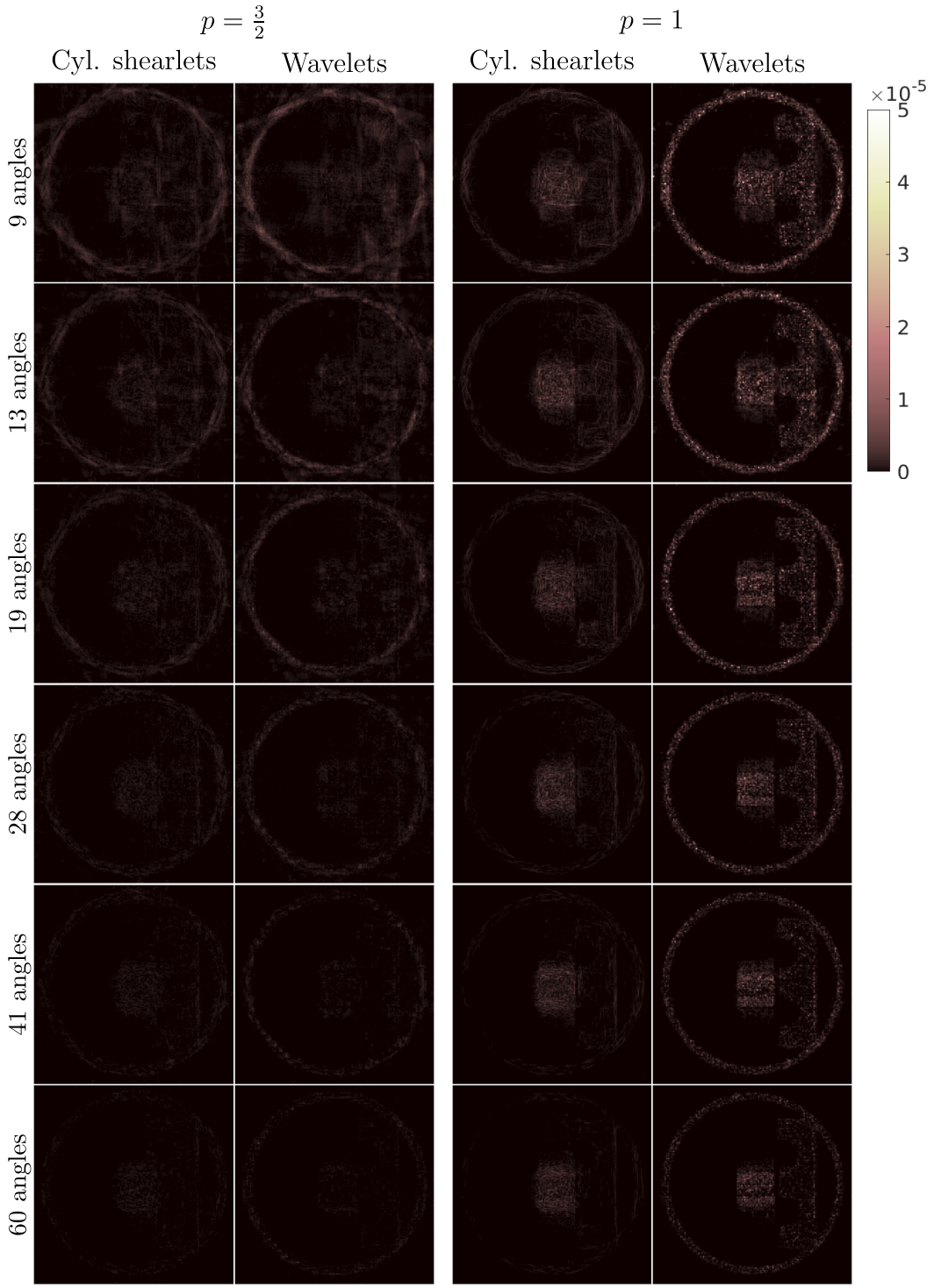

Figure SM6. *Pixelwise variance between 5 reconstructions samples of the STEMPO data. Columns show different regularization methods and p-norms, rows show different number of projection angles N. Only the results from time step $\tau = 7$ and fixed noise are shown.*